PREDICTING LOAD-CARRYING CAPACITY OF DOVETAIL CONNECTIONS USING THE STOCHASTIC FINITE ELEMENT METHOD

*G. Y. Jeong**

Assistant Professor
Department of Wood Science and Engineering
Chonnam National University
77 Yongbongro Bukgu
Gwangju 500-757, Korea
E-mail: gjeong1@chonnam.ac.kr

M. J. Park

Director
E-mail: mjpark@forest.go.kr

J. S. Park

Research Scientist
Korea Forest Research Institute
57 Hoegiro, Dongdaemun-gu
Seoul 130-712, Korea
E-mail: jusang@forest.go.kr

K. H. Hwang

Senior Researcher
Korea Forestry Promotion Institute
1653 Sangamdong, Mapogu
Seoul 121-904, Korea
E-mail: khwang@kofpi.or.kr

(Received March 2012)

Abstract. The goal of this study was to evaluate the load-carrying capacity of dovetail connections. Different tenon angles (θ), tenon neck widths (w_1), tenon head widths (w_2), and tenon heights (h) were used to analyze stress distribution and strength from dovetail connections using the finite element method (FEM). Although different stress distributions were found from the FEM models, shear and tension perpendicular to the grain stresses were found to be the most critical stresses controlling strength of the dovetail connection. Strength of the dovetail connection predicted from the deterministic FEM models was validated from the results of experimental tests. A combination of four geometric parameters for mortise and tenon from the dovetail connection maximizing load-carrying capacity was found. Allowable load-carrying capacity of the dovetail connection was estimated using the stochastic finite element method associated with allowable stress design and load resistance factor design concepts.

Keywords: Dovetail connection, stress, stochastic finite element method.

INTRODUCTION

Dovetail connections are commonly used for traditional wood frame buildings in Korea. The dovetail connection is a type of wood-to-wood connection, the strength of which is based on the mechanical properties of material used and the fitness of tenon and mortise in the connection (Tannert et al 2010, 2011). The design of the dovetail connection used to be entirely dependent on skilled carpenters who learned through apprenticeship. With the advent of advanced

* Corresponding author

cutting machines, various geometries of dovetail connections are now available to architects. However, there are no guidelines for designing dovetail connections, which prevents the use of dovetail connections in modern buildings.

Evaluating dovetail connection strength is difficult because of the hierarchical structure and direction-dependent property of wood. A simplified approach and controllable assumptions are key aspects to simulating dovetail connections. Stress distributions associated with different tenon and mortise geometries could lead to quantifying failure behaviors of dovetail connections. With known failure modes associated with the stress distribution, critical factors could be identified and used for predicting strength and optimizing geometry of dovetail connections. If variations of material properties used for the dovetail connections are known, variations of load-carrying capacity for the connection could be estimated. Based on the relationship, allowable load-carrying capacity for the connection could also be found.

Jeong et al. (2010) measured orthotropic properties of loblolly pine (*Pinus taeda*) strands. Loblolly pine strands as a natural material and its material properties were quantified as a specific distribution. Different elastic modulus, strength, and failure behaviors in the longitudinal, radial, and tangential directions were found, which was highly related with anatomical structures. Jeong and Hindman (2009) also investigated mechanical behavior of differently oriented strands using stochastic finite element methods (SFEM). Although all wood specimens showed brittle failure behavior, differently oriented strands showed different stress distribution. Strength of differently oriented strands was predicted using Tsai-hill failure criteria. Sensitivity analysis showed that earlywood and latewood from the differently oriented strands participated in different proportions in terms of load-carrying capacity.

Tannert et al (2010, 2011) investigated mechanical behavior of rounded dovetail connections through experiments and the finite element method (FEM). Bending test results showed that failure behavior of the dovetail connection was brittle. The failure location of the rounded dovetail connection predicted from FEM was matched with the location observed from the experimental test. The modified Hashin criterion was applied to predict strength of the rounded dovetail connection.

Pang et al (2011) investigated effects of the crossing beam shoulder on the moment carrying capacity of the dovetail connection. With the increment of beam shoulder width, maximum moment of the dovetail connection increased. Failure behavior of the dovetail connection was also varied in association with the crossing beam shoulder width. When the crossing shoulder width was less than 50% of the crossing beam width, failure occurred at the mortise area of the post. When the crossing shoulder width was greater than 50% of the crossing beam width, a tension perpendicular to the grain failure occurred at the crossing beam shoulder.

Mose and Prion (2004) used FEM to predict mechanical properties of single bolted connections. Different combinations of panel type, end distance, edge distance, bolt diameter, and direction of loading were used to analyze ultimate load, ultimate displacement, and failure mode of single bolted connections. Weibull's weakest link theory and maximum stress theory were used to count stress concentration, probability of failure, and material variability. The difference of ultimate load between the predicted result from FEM and the experimental test ranged from 1-51%.

Sangree and Schafer (2009) applied FEM to predict load-carrying capacity of the traditional timber scarf joint. Two specific failure modes including shear parallel to the grain and tension perpendicular to the grain were identified. Hankinson's formula was used to predict strength of a scarf joint subjected to combined bending and tension.

Park et al (2010) investigated the effects of tenon neck width, tenon head width, tenon length, and tenon angle on the dovetail connection. Four tenon neck widths of 15, 20, 35, and 50 mm; two tenon

lengths of 30 and 45 mm; and four tenon angles of 15, 20, 25, and 30° were used to investigate effects of geometry on tensile strength of the dovetail connection. Based on experimental tests, a tenon neck width of 20 mm, a tenon neck length of 30 mm, and a tenon angle of 15-30° were recommended for designing the dovetail connection. However, it appears insufficient to provide a geometry parameter optimization for the dovetail connection based on a limited number of experimental tests.

Although previous studies showed that the structure of materials and failure behaviors are critical to predict strength of materials, effects of variation of material properties and geometric parameters on mechanical behavior of dovetail connections were not considered. Also, a design concept for the structural use of dovetail connections was not incorporated in predicting mechanical behavior of dovetail connections under a specific loading condition.

The goal of this study was to define the load-carrying capacity of dovetail connections under tension using SFEM. Different geometric parameters of tenon and mortise were evaluated to maximize the strength of the dovetail connection. Allowable stress design (ASD) and load resistance factor design (LRFD) concepts including consideration for the specific type of loading condition, failure mode, material resistance value, and resistance variability were incorporated with SFEM to simulate load and resistance distribution and predict design value for the dovetail connection (AFPA 1996, 2005).

METHODS

Constructing the Dovetail Connection Using the Finite Element Method

Figure 1 shows the dovetail connection including different geometric parameters for mortise and tenon. Different geometries of mortise and tenon from the dovetail connection were constructed using FEM. Four node quad elements with the plane strain assumption were applied to simulate mechanical behavior of the dovetail connection under tension. The beam was 150 mm wide and 1000 mm long. As Eq 1 shows, the geometries of mortise and tenon could be defined by the relationship of four factors: tenon head width (w_2), tenon neck width (w_1), tenon height (h), and tenon angle (θ).

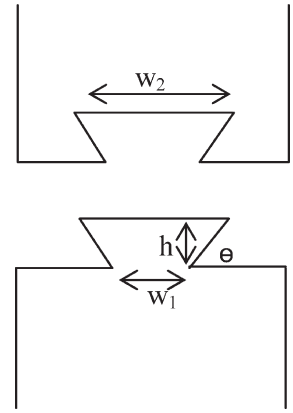

Figure 1. Dovetail connection with four geometric variables for tenon and mortise.

Different friction coefficients from 0.3-0.6 for wood-to-wood connections were investigated. With the increment of the friction coefficient from 0.3-0.6, tension stress in the y direction decreased 4.1%, shear stress decreased 2.7%, and compression stress decreased 13.9%. Although the friction coefficient influenced the stress distribution of wood-to-wood connections, a friction coefficient of 0.3 was applied to check the most critical case.

$$\sin\theta = \left(\frac{h}{\sqrt{\left(\frac{w_2 - w_1}{2}\right)^2 + h^2}} \right) \qquad (1)$$

where θ is tenon angle, h is tenon height, w_1 is tenon neck width, and w_2 is tenon head width.

Model Input

Table 1 shows the different material properties and fitted distributions used as inputs for the dovetail connection models. Transverse isotropic assumption was applied including longitudinal elastic modulus (E_Y) of 11.3 GPa, transverse

Table 1. Average material properties and specific distributions used as input variables for deterministic FEM and SFEM models.

Material property	Estimated average value (GPa)	Estimated standard deviation (GPa)	Predicted average value (GPa)	Predicted standard deviation (GPa)	Fitted distribution	Scale	Shape	Theta
Longitudinal elastic modulus	11.3000	4.16000	11.3400	4.06000	Weibull	12.69	3.05	0
Transverse elastic modulus	0.44000	0.18000	0.42000	0.18000	Weibull	0.48	2.48	0
Shear strength	0.01200	0.00219	0.01198	0.00252	Weibull	12.98	5.47	0
Radial strength	0.00423	0.00121	0.00425	0.00121	Weibull	4.69	3.90	0
Tangential strength	0.00280	0.00041	0.00280	0.00043	Weibull	2.98	7.70	0

FEM, finite element method; SFEM, stochastic finite element method.

elastic modulus (E_X) of 0.44 GPa, shear modulus (G_{XY}) of 0.7 GPa, and Poisson's ratio (ν_{XY}) of 0.038 to represent the material property of glulam. E_Y and E_X were determined from the tension test, and shear modulus and Poisson's ratio were assumed based on elastic ratios (Bodig and Goodman 1973). Shear and transverse strength were determined from shear block and tension tests, respectively.

Deterministic FEM was used to analyze effects of geometric factors on mechanical behavior of dovetail connections. Average elastic modulus and strength values from Table 1 were used for the deterministic FEM models. Different combinations of four geometric variables obtained from Eq 1 were used to investigate effects of the geometric parameters on stress values. Note that the variables shown in Table 2 were not used as a combination. It showed all the lists for each representative parameter used for the investigation. From the FEM results, a combination of four geometric variables that allowed the dovetail connection to carry the highest load was defined.

Table 2. Different geometric factors for tenon and mortise in the dovetail connection.

Tenon angle (θ, degrees)	Tenon neck width (w_1, mm)	Tenon head width (w_2, mm)	Tenon height (h, mm)
80.57	88.16	32.55	41.22
71.60	78.16	36.19	39.84
63.46	68.16	39.83	38.47
56.33	58.16	43.47	37.10
50.21	48.16	47.11	35.72
45.02	38.16	50.74	34.35
40.62	28.16	54.38	27.48
36.88	18.16	58.02	20.61
33.70	8.16	61.66	13.74
30.97		65.30	
28.62		68.94	
26.57		72.58	
		76.22	

Regardless of different geometries, dovetail connections failed in a brittle manner (Park et al 2010). Therefore, maximum stress of the dovetail connection can be considered as a function of load because of the lack of nonlinear deformation. With known maximum strength values from the experimental results (Hwang and Park 2008; Park et al 2010), stress values obtained from FEM models could be used to calculate dovetail connection strength. From the slope of the stress and load relationship, the stress components could be summarized as a function of load and slope for the stress components (Jeong and Hindman 2009). Based on the experimental and simulation results, the most critical failures of the dovetail connection were found to be governed by shear and tension perpendicular to the grain. The failure criterion for the material should reflect failure behaviors of materials (Jeong and Hindman 2009). Therefore, a practical failure criterion could be defined as follows:

$$\frac{\sigma_{tpe}}{T_{pe}} + \frac{\tau_{xy}}{S} - 1 \leq 0 \qquad (2)$$

where σ_{tpe} is tension perpendicular to the grain stress, τ_{xy} is shear stress, T_{pe} is tension perpendicular to the grain strength, and S is shear strength.

Two stress components, tension perpendicular to grain stress (σ_{tpe}) and shear stress (τ_{xy}) values, were obtained from FEM models, and two strength indices, tension perpendicular to grain strength and shear strength, were obtained from

experimental tests. To validate the FEM models, failure loads determined from experimental tests and failure loads predicted from FEM models were compared.

Probabilistic SFEM models were used to analyze allowable load-carrying capacity for dovetail connections with the four geometric variables defined from the FEM model carrying the highest load. Fitted distributions of material properties with specific parameters from Table 1 were used for the SFEM model. One thousand loops were executed to generate random elastic modulus values and strength indices based on specific distributions from Table 1 using Monte Carlo simulation associated with the Latin Hypercube Sampling technique. With the distributions of stress components from SFEM and distributions of strength indices from experimental tests, probabilistic failure loads were predicted to be associated with ASD and LRFD.

According to ASTM (2007, 2010, 2011), design loads for dovetail connections were calculated. In ASD, a design tension load can be derived using a lower percentile load of 5% divided by an adjustment factor of 2.1 for tension and shear. Incorporating design strength for Tpe_{ASD} and S_{ASD} with stress components from the SFEM model, allowable load-carrying capacity of the dovetail connection based on ASD could be calculated with Eq 3. In LRFD, demand and capacity for the dovetail connection could be expressed as factored resistance values ($\lambda\varphi_z Z'$) and required connection resistance values (Z_u) from Eq 4. The factored resistance values of the dovetail connection could be divided into the two critical stress cases in Eq 2 and incorporated with the time effect factor (λ) and the resistance factor for the two stress cases. Maximum load-carrying capacity based on LRFD could be calculated with Eq 5.

$$\frac{\sigma_{tpe}}{T_{pe\ ASD}} + \frac{\tau_{xy}}{S_{ASD}} \leq 1.0 \quad (3)$$

$$\lambda\phi_z Z' \geq Z_u \quad (4)$$

$$\frac{\sigma_{tpe}}{\lambda\phi_t Tpe'} + \frac{\tau_{xy}}{\lambda\phi_s S'} \leq 1.0 \quad (5)$$

where Tpe_{ASD} is tensile perpendicular to the grain strength divided by 2.1, S_{ASD} is shear strength divided by 2.1, λ is time effect factor (0.6), ϕ_t is resistance factor for tension, ϕ_s is resistance factor for shear, Tpe' is the adjusted tension perpendicular to the grain resistance, and S' is adjusted shear resistance.

RESULTS AND DISCUSSION

Table 3 shows percentage difference comparisons between average failure loads of dovetail connections from experimental tests (Park et al 2010) and average failure loads predicted from the FEM models. Results showed that the difference between experimental results and FEM model results ranged from 3.4-20.8%. Considering the variability of materials, the FEM models predicted failure loads of the dovetail connection very well. With the validated FEM models, more systematic analysis of geometric variable effects on stress distribution and load-carrying capacity of the dovetail connection could be achieved.

Comparison among Stress Distributions and Failure Modes for Dovetail Connections

Figure 2 shows the different stress distributions from simulation and typical failure behaviors of

Table 3. Difference between failure load from experimental test and failure load from deterministic FEM models.

Geometric variables						
Tenon angle, θ (degrees)	h (mm)	w_1 (mm)	w_2 (mm)	Failure load from experimental, kN (COV)	Failure load from FEM (kN)	Difference (%)
60	30	20.36	55	18.3 (15.8)	20.4	11.4
75	30	15.92	32	14.4 (13.5)	11.4	20.8
65	30	19.02	47	20.2 (18.9)	16.8	16.8
75	45	35.89	60	11.7 (14.6)	11.3	3.40

FEM, finite element method.

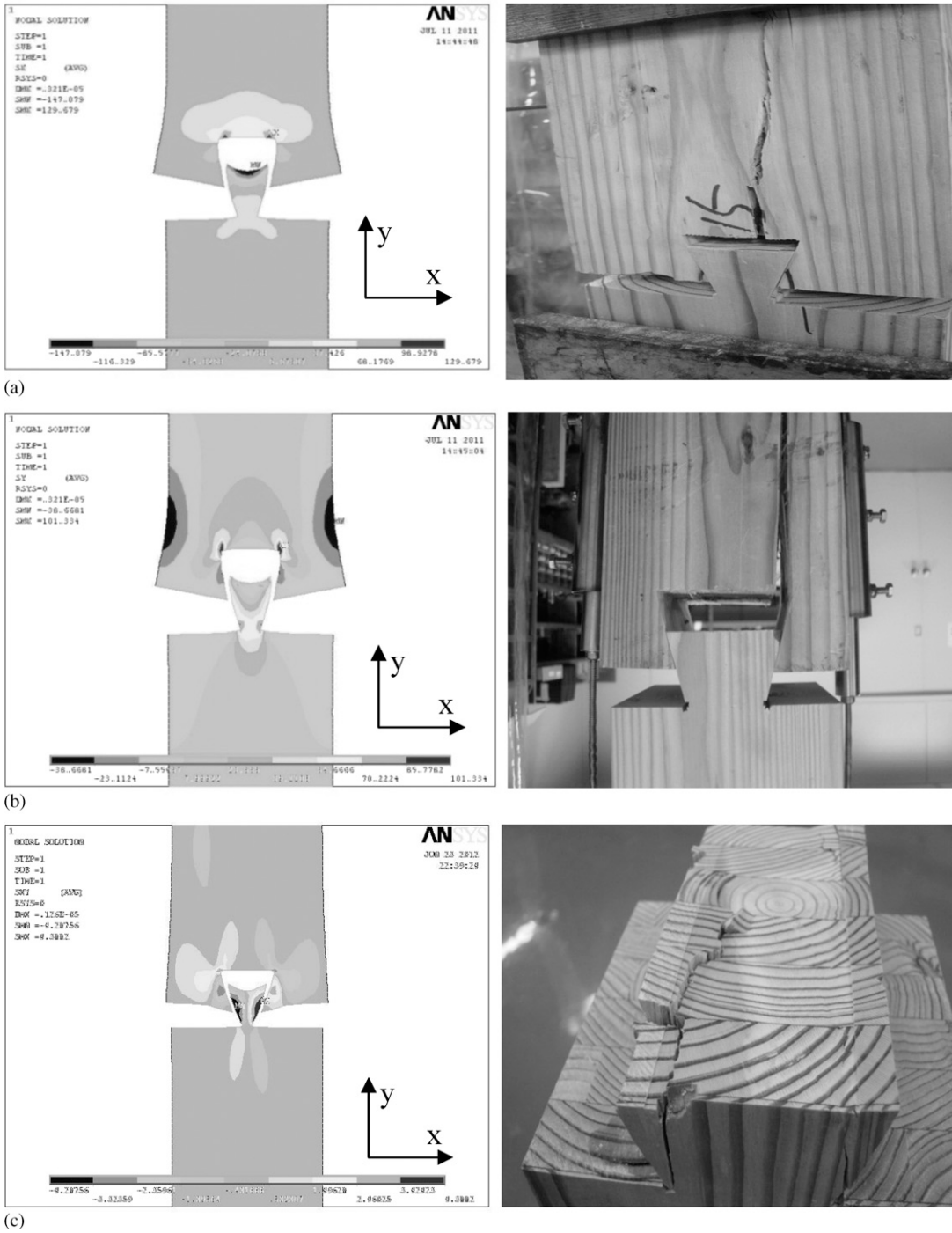

Figure 2. Different failure behaviors of the dovetail connection: a) transverse stress x distribution from a FEM model and a tension perpendicular to the grain failure at mortise, b) longitudinal stress y distribution from a FEM model and a shear failure at mortise, and c) shear stress distribution from a FEM model and a shear failure along the side of the tenon. FEM, finite element method.

the dovetail connection from experimental tests. Stress distributions from simulation captured various failure modes of the dovetail connection. Figure 2a shows stress x distribution, which is the normal stress perpendicular to the grain. Although the highest compression stress value in the x direction occurred at the head of the tenon, the highest tension stress value in the x direction occurred at the mortise. Because strength of wood in tension perpendicular to the grain was weakest, the ultimate failure occurred at the mortise area observed from the experimental test. Figure 2b shows stress y distribution, which is the longitudinal stress. The highest stress occurred at the reentrant corner of the mortise, whereas compression stress occurred under the re-entrant corner of the mortise. These stress distributions created shear between fibers. Figure 2c shows the shear stress distribution. Maximum shear stress occurred along the side of the tenon. Experimental test results showed that the side of the tenon failed along the shear plane. This failure mode occurred because tension force created shear between fibers along the longitudinal direction. A previous study showed that shear strength of glulam ranged from 9.6-13.0 MPa (Hwang and Park 2008). Compared with normal strength in the longitudinal direction of the glulam, shear strength of the glulam was 4.3 times lower. Keenan (1974) found that shear strength of Douglas-fir glued–laminated beams depended on the sheared area. Considering the strength ratios of the glulam material from Table 1 and stress distributions in Fig 2, critical failure modes of the dovetail connection were dominated by either tension perpendicular to grain stress or shear stress.

Changes of Tension Perpendicular to Grain Stress and Shear Stress Associated with Geometric Variables of Tenon and Mortise in the Dovetail Connection

Different tenon angles, tenon head widths, tenon neck widths, and tenon heights were derived from Eq 1 to analyze the effects of the geometric variables on stress values of the dovetail connection. Figure 3a shows changes of tension perpendicular

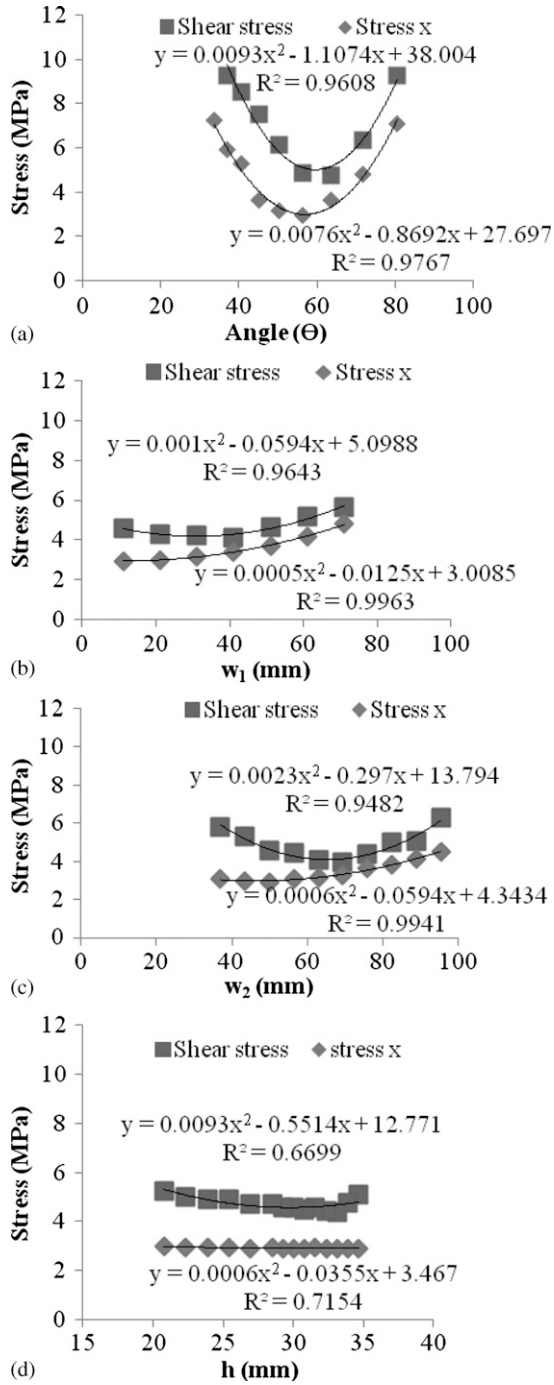

Figure 3. Change of tension perpendicular to the grain stress and shear stress in dovetail connection with the increment of geometric variables: (a) the tenon angle (θ), (b) tenon neck width (w_1), (c) tenon head width (w_2), and (d) tenon height (h).

to the grain stress and shear stress values around the tenon and mortise area when tenon angle increased at a tenon height of 30 mm and a tenon neck width of 20 mm. The increment of the tenon angle changed the tenon head width with a tenon height and a tenon neck width according to Eq 1. Because of the geometric relation, the tenon angles from 80.57-33.70° were investigated, which produced the corresponding tenon head widths from 30-110 mm. With the change of tenon angle, tension stress x, and shear stress, xy showed a parabolic curve. The complicated stress values were calculated associated with the friction and bearing area between the tenon and mortise. The lowest shear stress of 4.75 MPa occurred at a tenon angle of 63°. The lowest tension stress x of 2.92 MPa occurred at a tenon angle of 56°. Considering the fact that failure of the dovetail connection was controlled by two mixed stress values, the optimum tenon angle for maximizing load capacity could range from 56-63°.

Figure 3b shows the change of tension perpendicular to the grain stress and shear stress values around the tenon and mortise area when tenon neck width increased at a tenon angle of 57° and a tenon height of 30 mm. With the change of tenon neck width, tension perpendicular to the grain stress and shear stress showed a different trend. Although shear stress at the tenon area showed a parabolic curve with the increment of tenon neck width, tension perpendicular to the grain stress increased. The lowest shear stress of 4.09 MPa occurred when tenon neck width was 41 mm. Tension perpendicular to the grain stress increased as tenon neck width increased. The lowest tension perpendicular to the grain stress of 2.90 MPa occurred when tenon neck width was 11.04 mm.

Figure 3c shows the change of stress values associated with tenon head width given a tenon angle of 57° and a tenon neck width of 11 mm. Although shear stress showed a parabolic curve with the increment of tenon head width, tension perpendicular to the grain stress increased gradually. The lowest tension perpendicular to the grain stress, 2.92 MPa, was found when tenon head width was 49.95 mm. The lowest shear stress, 3.92 MPa, occurred when tenon head width was 69.43 mm. With a consistent tenon angle and tenon neck width, tension perpendicular to the grain stress increased associated with the increment of tenon head width and tenon height. Therefore, optimum tenon head width should range from 49.95-69.43 mm. Considering the fact that tension perpendicular to the grain stress was the most critical stress that controlled the strength of the dovetail connection, tenon head width should be close to 49.95 mm to minimize the stress value.

Figure 3d shows the change of tension perpendicular to the grain stress and shear stress values associated with tenon height given a tenon angle of 57° and a tenon head width of 50 mm. Tension perpendicular to the grain stress and shear stress showed different trends with increment of tenon height. When tenon height increased, shear stress decreased until the tenon height reached 33 mm but sharply increased after tenon height was greater than 33 mm. However, tension perpendicular to the grain stress was almost not changed with increment of tenon height. The lowest shear stress, 4.38 MPa, occurred at tenon height 33.11 mm. Because tension perpendicular to the grain stress did not vary with increment of tenon height, the shear stress value associated with tenon height could be used to maximize the load-carrying capacity of the dovetail connection. Considering the ratio of shear stress to the tension perpendicular to the grain stress, a tenon height of 33.11 mm was found to maximize the load-carrying capacity of the dovetail connection associated with a tenon angle of 57°, a tenon head width of 50 mm, and a tenon neck width of 7 mm. The average load-carrying capacity for the dovetail connection with the four geometric variables was calculated to be 21.4 kN. The determined combination of four geometric variables from the deterministic FEM model was used to calculate allowable load-carrying capacity for the dovetail connection.

Allowable Tension Load for Dovetail Connections

Figure 4 shows load and resistance distribution from ASD, LRFD soft conversion, and LRFD hard conversion. The overlap zone indicates the region in which the load was higher than the resistance of the dovetail connection. In other

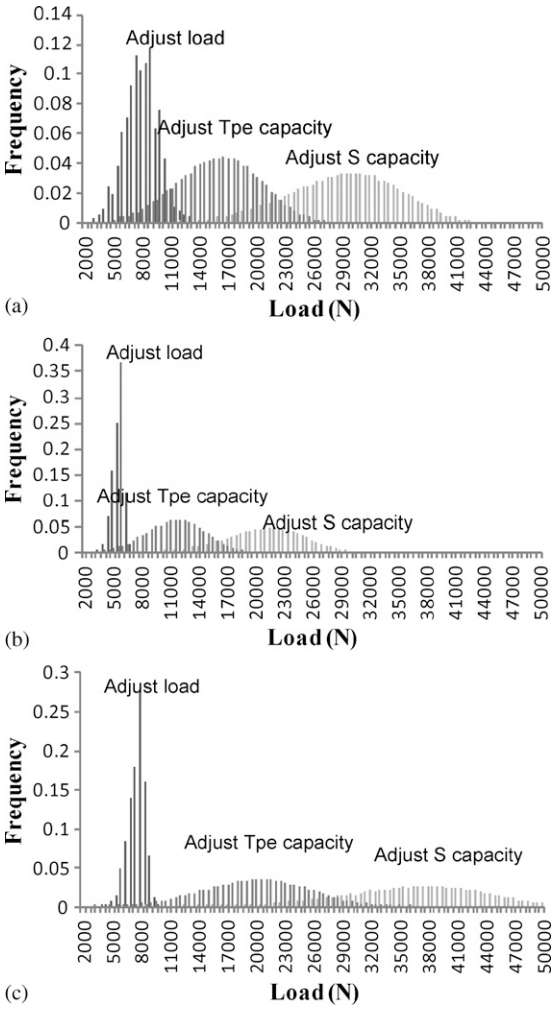

Figure 4. Load and resistance distribution: (a) load and resistance distribution from ASD; (b) load and resistance distribution of LRFD soft conversion from ASD; (c) load and resistance distribution of LRFD hard conversion. ASD, allowable stress design; LRFD, load resistance factor design.

words, the overlap zone is the failure region. The greatest failure region was observed from the distribution of load and resistance based on ASD, whereas the smallest failure region was observed from the LRFD hard conversion.

For ASD, the load distribution ranged from 1.05-11.92 kN, the adjusted tension perpendicular to the grain stress ranged from 1.92-27.84 kN, and the adjusted shear strength ranged from 6.18-45.93 kN. Allowable tension perpendicular to the grain stress of 1.22 MPa and allowable shear stress of 3.77 MPa were used to calculate the allowable tension load-carrying capacity of the dovetail connection using Eq 3.

For LRFD soft conversion, the load distribution ranged from 2.37-6.45 kN, resistance for tension perpendicular to the grain ranged from 1.36-19.73 kN, and resistance for shear ranged from 4.38-32.55 kN. A format conversion factor, K_F, of 2.88 from ASTM (2010) for shear and tension perpendicular to the grain strength was used to calculate the adjusted shear strength and tension perpendicular to the grain strength values. The same resistance factor of 0.75 for tension perpendicular to the grain strength and shear strength was used. A factored resistance value ($\lambda\varphi_z Z'$) of 1.35 MPa for tension perpendicular to the grain strength and a factored resistance value ($\lambda\varphi_z Z'$) of 4.65 MPa for shear strength were used to estimate design tension load-carrying capacity of the dovetail connection using Eq 5.

For LRFD hard conversion, the load distribution ranged from 3.32-9.10 kN, resistance for tension perpendicular to the grain stress ranged from 2.42-35.14 kN, and resistance for shear stress ranged from 7.80-57.97 kN. Data confidence factors for tension perpendicular to the grain strength of 0.89 and shear strength of 0.849 were obtained from ASTM (2010). The same computed resistance factor of 1.1254 for tension perpendicular to the grain stress and shear stress were calculated based on ASTM (2010). A factored resistance value ($\lambda\varphi_z Z'$) of 1.88 MPa for tension perpendicular to the grain strength and a factored resistance value ($\lambda\varphi_z Z'$) of 6.80 MPa for shear strength were used to estimate the tension load-carrying capacity of the dovetail connection using Eq 5. The allowable tension load-carrying capacity values of the dovetail connection were estimated to be 3.95 kN for ASD, 4.88 kN for the LRFD soft conversion, and 6.88 kN for the LRFD hard conversion. Allowable load-carrying capacity of the dovetail connection from SFEM associated with ASD was found to be the most conservative for designing the dovetail connection, whereas the load-carrying capacity of the dovetail connection

from SFEM associated with LRFD hard conversion was found to have the highest design value. When reliable information on the material property and load case is available, the LRFD hard conversion could produce a higher design value regarding the dovetail connection compared with ASD, which used an ambiguous safety factor.

CONCLUSIONS

This study investigated the effects of geometric variables on mechanical behavior of the dovetail connection and estimated the allowable load-carrying capacity of the dovetail connection. From the deterministic FEM models, different stress distributions associated with geometric parameters of the dovetail connection occurred. Critical shear stress occurred along the side of the tenon. Critical normal stress occurred at the re-entrant corner of the mortise. Critical tension perpendicular to the grain stress occurred around the mortise area. These stress distributions from the FEM models were matched with failure behaviors of the dovetail connection from experimental tests. Failure modes of the dovetail connection were dominated by tension perpendicular to the grain stress and shear stress. The proposed failure criteria associated with the critical stresses were found to be effective at predicting load-carrying capacity from the dovetail connection.

Based on the FEM results, dovetail connections with a tenon angle of 57°, a tenon neck width of 7 mm, a tenon head width of 50 mm, and a tenon height of 33 mm were found to carry the highest tension load. The allowable load-carrying capacity of the dovetail connection was estimated using SFEM associated with ASD and LRFD concepts. The design tension load-carrying capacity values of the dovetail connection were estimated to be 3.95 kN for ASD, 4.88 kN for LRFD soft conversion, and 6.88 kN for LRFD hard conversion.

ACKNOWLEDGMENTS

This study was financially supported by Korea Forest Research Institute and Chonnam National University.

REFERENCES

AFPA (1996) Standard for load and resistance factor design for engineered wood construction. American Forest and Paper Association, Washington, DC.

AFPA (2005) National design specification for wood construction. American Forest and Paper Association, Washington, DC.

ASTM (2007) D 1990-07. Standard practice for establishing allowable properties for visually-graded dimension lumber from in-grade tests of full-size specimens. American Society for Testing and Materials, West Conshohocken, PA.

ASTM (2010) D 5457-10. Standard specification for computing reference resistance of wood-based materials and structural connections for load and resistance factor design. American Society for Testing and Materials, West Conshohocken, PA.

ASTM (2011) D 245-06. Standard practice for establishing structural grades and related allowable properties for visually graded lumber. American Society for Testing and Materials, West Conshohocken, PA.

Bodig J, Goodman JR (1973) Prediction of elastic parameters for wood. Wood Sci 5(4):249-264.

Hwang KH, Park JS (2008) Estimation of moment resisting property for pin connection using shear strength of small glulam specimens. Mokchae Konghak 36(4):58-65 [in Korean with summary in English].

Jeong GY, Hindman DP (2009) Ultimate tensile strength of loblolly pine strands using stochastic finite element method. J Mater Sci 44(14):3824-3832.

Jeong GY, Hindman DP, Zink-Sharp A (2010) Orthotropic properties of loblolly pine (*Pinus taeda*) strands. J Mater Sci 45(21):5820-5830.

Keenan FJ (1974) Shear strength of wood beams. Forest Prod J 24(9):63-70.

Mose DM, Prion HGL (2004) Stress and failure analysis of wood composites: A new model. Compos, Part B Eng 35(3):251-261.

Pang SJ, Oh JK, Park JS, Park CY, Lee JJ (2011) Moment-carrying capacity of dovetailed mortise and tenon joints with or without beam shoulder. J Struct Eng 137(7):785-789.

Park JS, Hwang KH, Park MJ, Shim KB (2010) Tensile performance of machine-cut dovetail joint with Larch glulam. Mokchae Konghak 38(3):1-6 [in Korean with summary in English].

Sangree RH, Schafer BW (2009) Experimental and numerical analysis of a halved and tabled traditional timber scarf joint. Construct Build Mater 23(2):615-624.

Tannert T, Lam F, Vallée T (2010) Strength prediction for rounded dovetail connections considering size effects. J Eng Mech 136(3):358-366.

Tannert T, Lam F, Vallée T (2011) Structural performance of rounded dovetail connections: Experimental and numerical investigations. Eur J Wood Wood Prod 69(3):471-482.